Article

Increasing hourly heavy rainfall in Austria reflected in flood changes

https://doi.org/10.1038/s41586-025-08647-2

Received: 4 June 2024

Accepted: 10 January 2025

Published online: 12 March 2025

Open access

Check for updates

Klaus Haslinger[1]✉, Korbinian Breinl[2], Lovrenc Pavlin[2], Georg Pistotnik[1], Miriam Bertola[3], Marc Olefs[1], Marion Greilinger[1], Wolfgang Schöner[4] & Günter Blöschl[3]

Climate change is expected to increase heavy rainfall with concomitant increases in flooding[1]. Causes of increased heavy rainfall include the higher water-holding capacity of a warmer atmosphere and changes in atmospheric circulation patterns[2], which may translate into future heavy rainfall increases in most of Europe[3]. However, gathering evidence on the time evolution of past changes has been hampered by data limitations and measurement uncertainties, in particular for short rainfall durations, such as 1 h. Here we show an 8% increase in daily and 15% increase in hourly heavy rainfall over the last four decades by analysing a new dataset comprising 883 stations in Austria from 1900 to 2023. These increases are fully consistent between two independent networks and occurred after a retarding phase between 1960 and 1980. Hourly heavy rainfall changes are aligned with temperature increases with the sensitivity of a 7% increase per 1 °C of warming, in line with Clausius–Clapeyron scaling. Daily heavy rainfall changes, however, are aligned with atmospheric circulation indices with little correlation to air temperature, which suggests a bigger role of atmospheric circulation modes than previously thought. The daily heavy rainfall changes are remarkably consistent with observed flood increases of about 8% in large catchments. The hourly heavy rainfall changes are similarly consistent with flood changes in small catchments, although the flood increase is stronger (25% over the last four decades). Climate adaptation measures in flood management may therefore be more pressing for rivers draining smaller catchment areas than for large rivers.

Heavy rainfall has become a matter of concern in recent years because of the major disruptions to human systems caused by flash floods, regional floods and landslides[4]. Climate change is expected to increase precipitation intensity on time scales from minutes to days, which will impact flooding[1,3,5]. Previous studies have shown that observed heavy rainfall occurring on a daily basis has increased in recent decades in many parts of the world[6]. Positive trends of 0.6–1.4% per decade have been found in Central Europe[7,8], but there is only moderate confidence in their robustness[1]. For sub-daily time scales, several observation-based studies point towards a relationship of heavy rainfall and temperature, suggesting an increase of about 7% per degree of warming. This percentage is consistent with the Clausius–Clapeyron relationship that describes an increase in the atmospheric water-holding capacity with temperature[2,9,10]. In some areas, such as the Netherlands, larger percentages have been determined, known as super scaling[11,12]. However, enhanced water-holding capacity is only one of the controls of increased heavy rainfall, and there are still discrepancies between observed trend magnitudes and changes in potential drivers[2]. This is mostly due to a lack of long, high-quality observations. Although recent progress has been made in compiling data[13], there is still very low confidence in the changes in hourly heavy rainfall[1]. Also, rain gauge instrumentation has changed in most countries of the world in the last few decades (floaters, tipping buckets, weighing gauges). Different error characteristics of the instruments may have masked any changes or given rise to apparent changes, depending on the error magnitudes[14,15].

Here we analyse the most comprehensive dataset of heavy rainfall in Austria from two independent networks, and show, with high confidence, that hourly heavy rainfall has been increasing since 1980, induced by climate change, and is closely reflected in increasing floods in small catchments.

Heavy rainfall observations

We based our analysis on rainfall observations from 883 rain gauge stations (779 stations with daily resolution, 163 with hourly resolution) (Extended Data Fig. 1a) from two completely independent measurement networks over the period 1900 to 2023. One network is operated by GeoSphere Austria (GSA, the National Meteorological Service of Austria) and the other by the Hydrographic Service of Austria (HYD). Comparison of the two datasets offered a unique opportunity to objectively assess the role of measurement uncertainty vis-à-vis real changes. The full history of instrument types is known, which allowed us to estimate likely changes in the measurement errors for both networks (Tables 1 and 2). Heavy rainfall was evaluated on

[1]Department for Climate Impact Research, GeoSphere Austria – Federal Agency for Geology, Geophysics, Climatology and Meteorology, Vienna, Austria. [2]Directorate for Water Balance, Federal Ministry Republic of Austria for Agriculture, Forestry, Regions and Water Management, Vienna, Austria. [3]Institute of Hydraulic Engineering and Water Resources Management, Vienna University of Technology, Vienna, Austria. [4]Department of Geography and Regional Sciences, University of Graz, Graz, Austria. ✉e-mail: klaus.haslinger@geosphere.at

Table 1 | Station years of daily and hourly rain gauge data for different registration types from the two networks in Austria

	Daily data		Hourly data	
	GSA	HYD	GSA	HYD
Ombrometer	3,158	74,524	–	–
Floater	–	–	307	3,172
Tipping bucket	990	103	1,722	775
Weighing gauge	328	259	149	1,617
Optical sensor	–	–	–	120

Table 2 | Systematic errors of daily and hourly heavy rainfall for different registration types of rain gauges

	Daily data	Hourly data
Ombrometer	±0%	–
Floater	–	−5%
Tipping bucket	−2.5%	−3%
Weighing gauge	−0.5%	−1%
Optical sensor	–	+20%

Negative errors indicate an underestimation of heavy rainfall, positive errors an overestimation. The effect of these errors on heavy rainfall evolution are shown in Extended Data Fig. 3.

a station-by-station basis as the 99th percentile in a moving 21-year window to detect the time evolution of low-frequency changes. We applied rigorous constraints on missing data and temporal coverage to assure robust results, and limited the analysis to the warm season (May to September), in line with data availability. Because rainfall extremes in the study region almost exclusively occur in the warm season[16,17], there was little loss of information.

To understand the process drivers of change, we compared the temporal evolution of heavy rainfall at daily and hourly scales with potential explanatory variables. For assessing the dynamic contribution, we used two indices of atmospheric circulation, representing meridionality and persistency of the atmospheric flow, derived from daily weather patterns as well as cyclone tracks. For assessing the thermodynamic contribution, we evaluated the instantaneous scaling and climate scaling of heavy rainfall with air temperature. There was little temporal co-occurrence of daily and hourly heavy rainfall (9.0 ± 0.4% overlap of days with hourly and daily heavy rainfall), so clear differences would be expected in the alignments of the process drivers with daily and hourly heavy rainfall. In addition, we compared the observed heavy rainfall evolution with observed warm season flood peak discharges in 693 catchments, ranging in size from 1 to 250,000 km² (Extended Data Fig. 1b).

Observed changes in heavy rainfall

Our data show a plateau of daily heavy rainfall in the first half of the twentieth century, lower rainfall in the 1970s and 1980s, a clear increase of about 8% from 1990 to 2010 and little change in the last decade (Fig. 1a). Hourly heavy rainfall at the 99th percentile indicates a low in the 1960s and 1970s, followed by a persistent increase of about 15% that extends to the end of the dataset in 2023 (Fig. 1b). The 99th percentiles shown in Fig. 1a,b correspond to rainfall intensities of around 30–70 mm d^{-1} and 6–16 mm h^{-1}, respectively (inset diagrams). The 90th and 99.9th percentiles increase by 12% and 18% in the last few decades, suggesting a somewhat stronger change, with increasing severity of the rainfall (Extended Data Fig. 2). The data from the two completely independent network operators (GSA and HYD) give fully consistent results, corroborating the validity of the observed changes in heavy rainfall at both the daily and hourly time scales. Accounting for changes in the registration type of the rain gauges increased the consistency between the networks (Extended Data Fig. 3). A transition from manual to tipping bucket gauges for the daily series from the GSA decreased the trends slightly because the latter had smaller biases. The transition from floaters to weighing gauges for the hourly series of the HYD also decreased the trends slightly.

There are clear differences in the evolution of the daily heavy rainfall changes between north and south of the European Alps (Fig. 1c). In the north, multidecadal variations are visible, with a low around 1980 and highs around 1940 and 2010, whereas in the south, the oscillations are somewhat weaker and are followed by an increase after 2000. This is consistent with the role of the European Alps as a clear climate divide in Europe, as has been shown in numerous studies[18,19]. The hourly heavy rainfall changes, however, are spatially consistent (Fig. 1d), with a plateau from 1950–1980 and a clear increase afterwards. There was little difference in the temporal evolution of either the daily or hourly heavy rainfall between high-elevation (above 800 m) and low-elevation (below or at 800 m) stations (Extended Data Fig. 5).

Attribution of heavy rainfall

To explain these multidecadal variations, we used a meridionality index and a persistency index as proxies for the dynamic contribution to change. These were derived from a daily weather-type classification covering Central Europe based on sea level pressure[20]. Air temperature was used as a proxy for the thermodynamic contribution. Daily heavy rainfall was significantly correlated with the proxies for the dynamic contribution, whereas hourly heavy rainfall was significantly correlated with the proxy for the thermodynamic contribution (Table 3).

The evolution of daily heavy rainfall in the north was well aligned with the meridionality index, with maxima around 1940 and 2010 and a minimum around the 1980s (Fig. 2a) (correlation coefficient $r = 0.77$, $P = 0.02$ in Table 3). Accounting for measurement biases had little effect on r (Extended Data Table 1). Several studies have shown the existence of multidecadal variations in meridional (south–north) atmospheric flow patterns in Europe related to spatial sea surface temperature gradients and Atlantic multidecadal variability[20–22]. Meridional flow patterns favour the formation of cut-off lows[23] and Vb cyclones[24], which approach the eastern Alps from the southwest and turn counter-clockwise. Both are conducive to heavy rainfall generation in Central Europe[8]. Vb cyclones had a high re-occurrence rate in the 1960s and 2010s, with a minimum during the 1980s[8], which is in line with the rainfall evolution illustrated in Fig. 2a (Extended Data Fig. 6a). The evolution of daily heavy rainfall in the north was also correlated ($r = 0.51$, $P = 0.10$) with the persistency index, and so was the daily heavy rainfall in the south (Fig. 2b) ($r = 0.61$, $P = 0.02$ in Table 3), which showed small variations from 1900 to 1990 and a clear increase after 1990. The increased persistency in the last few decades has been shown to be related to a decrease in the temperature difference between the mid-latitudes and the North Pole[25–27] and other factors[28–30]. Higher persistency implies more slowly moving storm systems and longer rainfall for a given area[31,32], which is reflected by the daily heavy rainfall increase in the south of about 7% since 1990. Other potential controls on daily heavy rainfall are sulfate aerosols, which tend to reduce heavy rainfall through their role in precipitation-forming processes, cloud microphysics and cloud dynamics[33–35]. Sulfate aerosols showed a pronounced peak in the 1970s, whereas the minimum in heavy rainfall occurred in the 1980s, and sulfate concentrations have been rather uniform in Europe while there has been a clear difference in daily heavy rainfall between the north and south. Thus, sulfate aerosols are unlikely a dominant driver of changes in daily heavy rainfall (Extended Data Fig. 6c,d).

The evolution of hourly heavy rainfall in both the north and south is very well aligned with air temperature, with a hiatus during the 1970s followed by a steep increase (Fig. 2c) ($r = 0.84$ and 0.94, $P = 0.04$ and

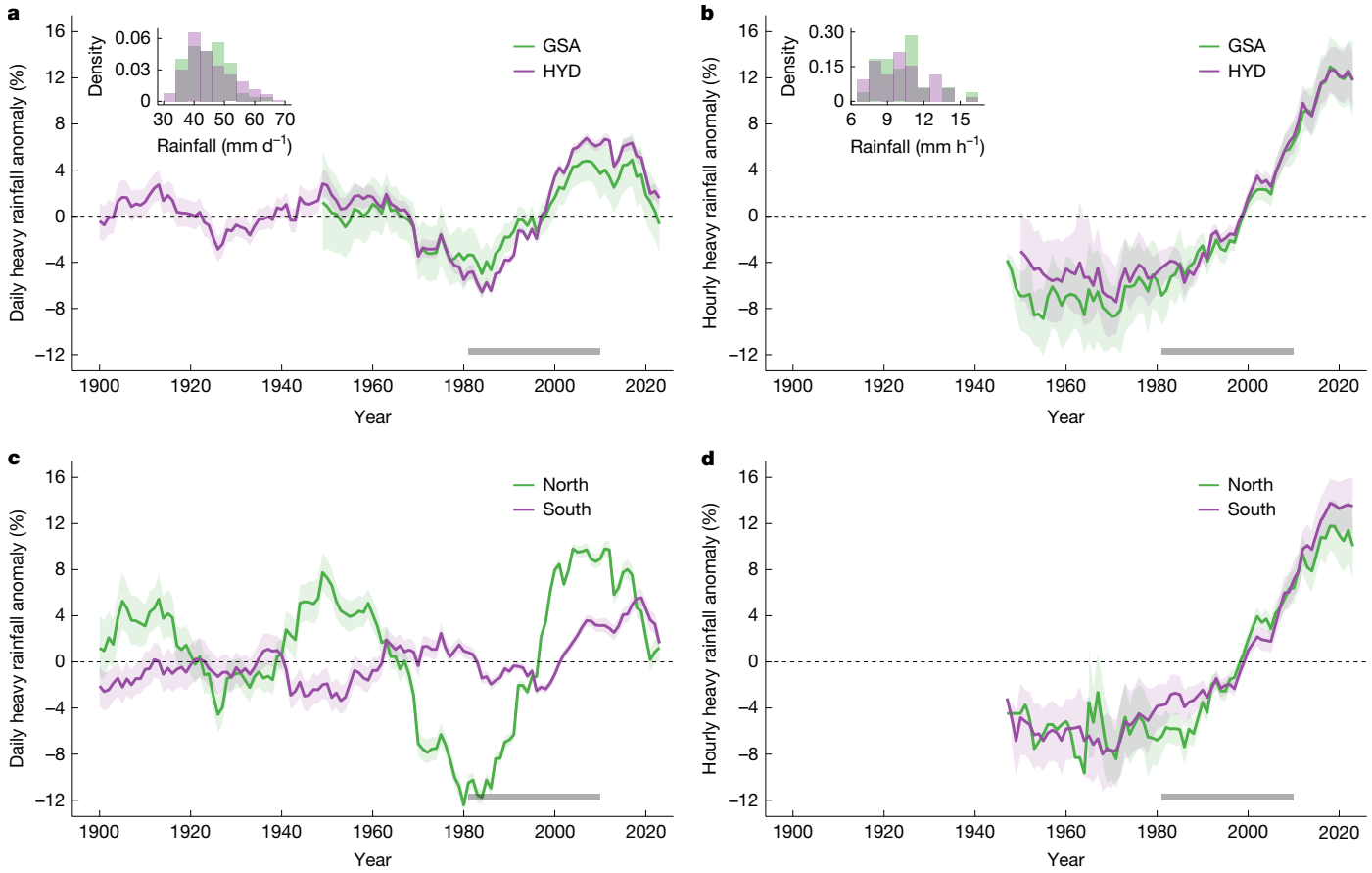

Fig. 1 | Heavy rainfall evolution in Austria. a, Daily heavy rainfall (99th percentiles of wet days) anomalies for the reference period 1981–2010 calculated from the GSA (green) and HYD (purple) datasets. Solid lines indicate the mean over all stations, shaded bands the 95% confidence interval of the mean estimated by bootstrapping (n = 1,000). The confidence intervals of the GSA data are wider because of the smaller number of stations. **b**, Hourly heavy rainfall (99th percentiles of wet hours) anomalies, otherwise similar to **a**. Insets, histograms of the 99th percentiles over all stations for 1981–2010. **c**, Daily heavy rainfall anomalies for north (green) and south (purple) of the Alpine ridge. **d**, Hourly heavy rainfall anomalies, otherwise similar to **c**. The grey bars at the bottom of each panel indicate the reference period.

0.03, respectively, in Table 3). Hourly rainfall extremes are almost entirely generated by convective processes, which are enhanced by the increased availability of water vapour, and hence latent energy, under higher air temperatures[2,36,37]. Convective storms are local phenomena that occur under a wide variety of different weather patterns, which explains the close alignment with temperature increases to both the north and south of the Alps. Binning the hourly heavy rainfall by air temperature on the same day (that is, instantaneous scaling) (Fig. 2d) showed an increase with air temperature of about 6.8 ± 0.1% °C^{-1}. This is what one would expect from the Clausius–Clapeyron relationship and, given the small change in relative humidity observed[38,39], a similar increase in specific humidity. The small differences in scaling between the north and south (Extended Data Table 3) may be related to the variety in weather patterns that produce extreme rainfall and the topographic complexity of the study region[40]. The average hourly heavy rainfall in the period 2003–2023 was 14.7% higher than that in the period 1950–1970 (Fig. 2e), and the average air temperature was 1.8 °C higher. These increases correspond to a climate scaling of 8.1 ± 1.2% °C^{-1}. The instantaneous and climate scaling of the hourly heavy rainfall were similar for different time periods and between the north and south (Extended Data Table 3).

The observed hourly heavy rainfall increases in recent decades in Austria are consistent between the two independent networks and are robust relative to measurement biases due to changed instrumentation over the years. The observed increases of 15% both north and south of the Alpine ridge over the last four decades are in line with observations from other parts of the world, such as increases of 10% and 11% in Denmark and China, respectively[41,42], and with the current understanding

Table 3 | Spearman's rank correlation coefficients of daily and hourly heavy rainfall with meridionality index, persistency index and air temperature for 1901–2020 (daily heavy rainfall) and 1947–2020 (hourly heavy rainfall)

	Daily heavy rainfall anomaly			Hourly heavy rainfall anomaly		
	Entire region	**North**	**South**	**Entire region**	**North**	**South**
Meridionality (dynamic)	**0.72 (0.02)**	**0.77 (0.02)**	−0.03 (0.92)	0.33 (0.40)	0.55 (0.13)	0.28 (0.48)
Persistency (dynamic)	**0.63 (0.04)**	0.51 (0.10)	**0.61 (0.02)**	0.27 (0.46)	0.48 (0.18)	0.25 (0.51)
Air temperature (thermodynamic)	0.22 (0.46)	0.27 (0.39)	0.27 (0.29)	**0.94 (0.03)**	**0.84 (0.04)**	**0.94 (0.03)**

P values in parentheses account for the autocorrelations of the time series[58]; significant correlations (P < 0.05) are in bold text. Analyses for the entire region and north and south of the Alpine ridge are separated.

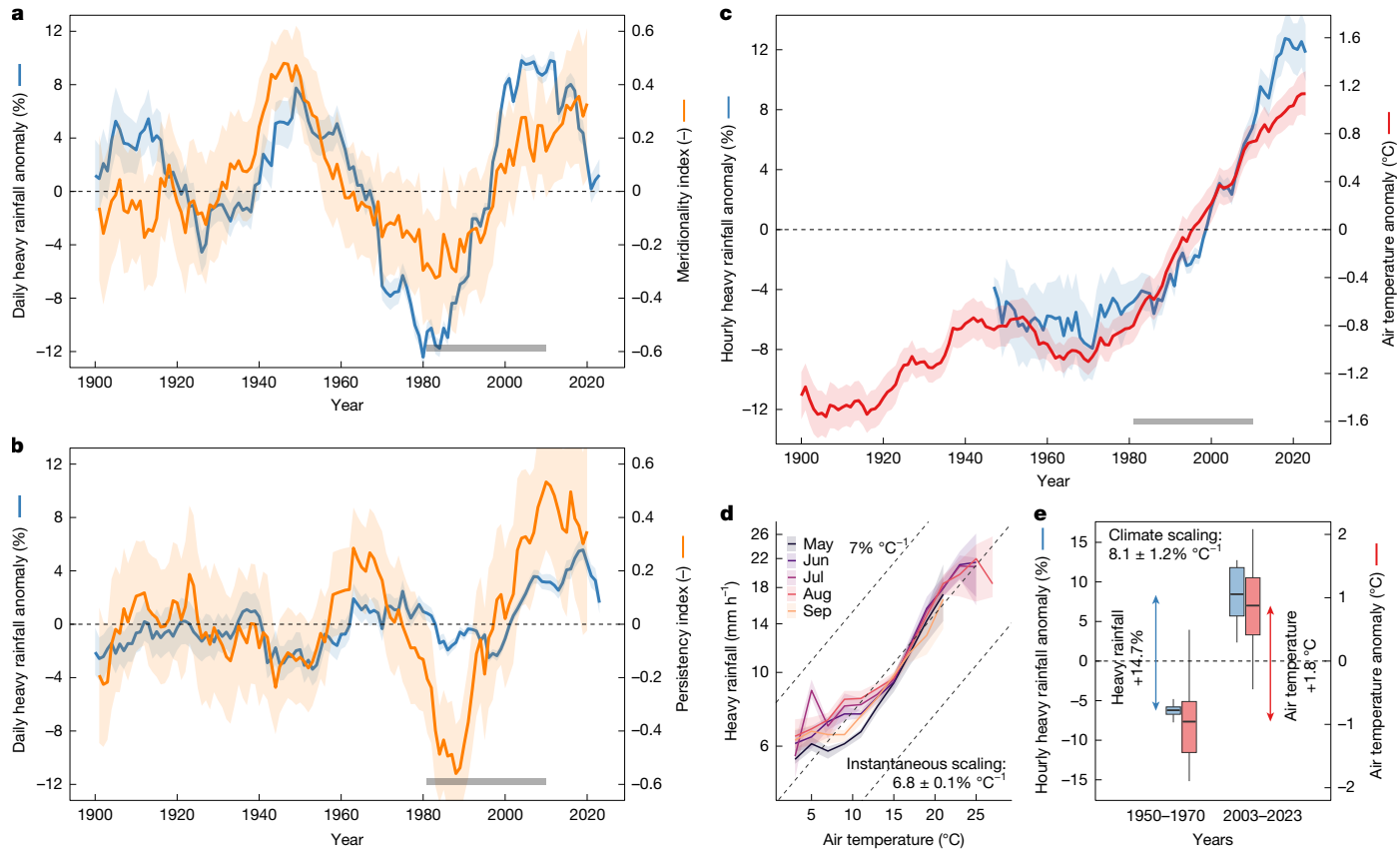

Fig. 2 | Attribution of heavy rainfall evolution in Austria. a, Daily heavy rainfall anomalies (both datasets) for the north and the meridionality index. **b**, Daily heavy rainfall anomalies (both datasets) for the south and the persistency index. **c**, Hourly heavy rainfall anomalies (both datasets) and air temperature anomalies over the entire domain. **d**, Instantaneous scaling: hourly heavy rainfall rates above the 99th percentile binned by daily air temperature of the day of occurrence for each month of the warm season. Grey dashed lines indicate scaling of +7% °C^{-1}. A quantile regression of (log-)hourly heavy rainfall against daily air temperature for 1950–2023 gives an instantaneous scaling across all months of 6.8 ± 0.1% °C^{-1}. **e**, Climate scaling: comparison of the periods 1950–1970 and 2003–2023. The average hourly heavy rainfall anomaly increases by +14.7% and the air temperature anomaly by +1.8 °C, which gives a climate scaling of 8.1 ± 1.2% °C^{-1}. The grey bars at the bottom of **a**–**c** indicate the reference period. The shaded bands in **a**–**d** indicate the 95% confidence interval of the mean, estimated by bootstrapping (n = 1,000). The lower and upper box boundaries in **e** are the 25th and 75th percentiles, respectively; the line inside the box is the mean; the upper and lower whiskers extend to the largest value, but no further than 1.5 times the interquartile range, and the points outside the whiskers are individual data points.

of extreme rainfall evolution in a warming climate[2,6,43]. The scaling of hourly heavy rainfall with air temperature of 7.0% °C^{-1} is also consistent with other regions, such as 8.5, 7.6 and 7.16% °C^{-1} in Australia, India and the United States, respectively[44]. The scaling found in this study is lower than the super scaling of about 14% °C^{-1} in the Netherlands[11], which may be related to the orographic effects of the Alps being more independent of temperature changes[45,46].

Daily heavy rainfall showed more marked decadal variations during the twentieth century than hourly heavy rainfall, and smaller increases in the last few decades. The decadal variations may explain some of the inconsistencies in the temporal trends reported in the literature[7]. Both the decadal variations and the recent increases in daily heavy rainfall are aligned with the dynamic contribution to rainfall changes, including a hiatus in the increase during the 1980s. The instantaneous scaling with air temperature is negative (−1.4% °C^{-1} north and −0.5% °C^{-1} south of the Alpine ridge for the period 1950–2023) (Extended Data Fig. 7 and Extended Data Table 3), implying no relevant thermodynamic contribution. The negative scaling rates are in line with those of other analyses of the same region[40], but contrast with those of other regions of the world where Clausius–Clapeyron scaling rates have been reported from (for example, 7 and 6.5% °C^{-1} in the Netherlands and the UK, respectively)[11,44,47]. The climate scaling found here was larger (2.4% °C^{-1} north and 2.2% °C^{-1} south of the Alpine ridge) (Extended Data Table 3) and possibly related to an alignment of the evolution of air temperature with that of the dynamic indices in the period 1985–2015. This alignment also resulted in a higher climate scaling for 1980–2000 versus 2003–2023 than for 1950–1970 versus 2003–2023 (6.9 and 2.6% °C^{-1}, respectively).

An important finding is that the daily heavy rainfall changes depend on atmospheric circulation patterns and therefore varied within the study region, whereas the hourly heavy rainfall changes are more locally driven by higher temperatures and, given that temperature is increasing more uniformly around the globe, seem to be more universal.

Implications for flood risk

Changes in heavy rainfall are expected to result in changes in flood magnitudes. Long rain storms tend to be most relevant in large catchments because of the long travel times of the water in the landscape, whereas shorter storms tend to be more relevant in smaller catchments. The time evolution of flood peak discharges in large catchments (areas greater than 500 km^2) is remarkably similar to that of daily heavy rainfall (Extended Data Fig. 8a). In the north (Fig. 3a), floods showed a similar hiatus around 1980 and a later increase of 25% (r = 0.67, P = 0.07) (Extended Data Table 2). In the south, the increases were smaller at 3%. There was also a clear correspondence between flood peak discharges in small catchments (areas less than 50 km^2) and hourly heavy rainfall (Extended Data Fig. 8b), but the increase in floods was greater than that of rainfall. In the north, floods have increased by about 30%, whereas

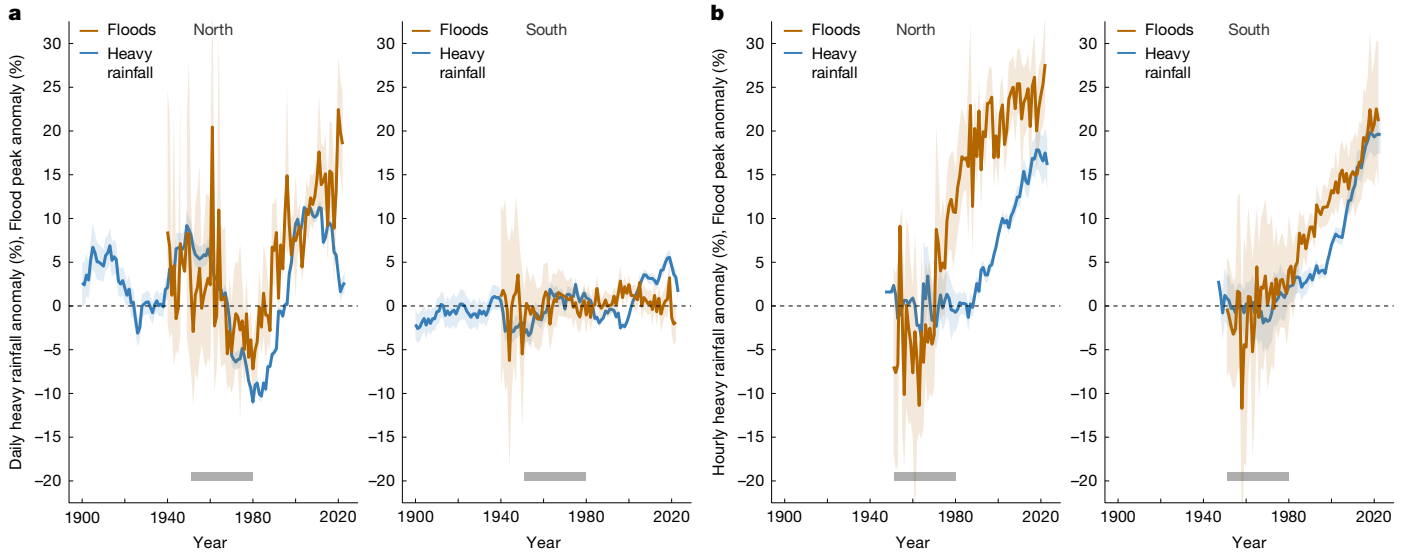

Fig. 3 | Effect of heavy rainfall evolution on flood peaks. a, Daily heavy rainfall anomalies and flood peak discharge anomalies for large catchments (greater than 500 km^2), north (left) and south (right) of the Alpine ridge. **b**, Hourly heavy rainfall anomalies and flood peak discharge anomalies for small catchments (less than 50 km^2), north (left) and south (right) of the Alpine ridge. Heavy rainfall values are 99th percentiles, as in Fig. 1, and flood peaks are the mean annual floods of the warm season. The grey bars at the bottom of the panels indicate the reference period. Solid lines indicate the mean over all stations, the shaded bands the 95% confidence interval of the mean, estimated by bootstrapping (n = 1,000). A remarkable similarity can be seen between the daily heavy rainfall and floods in large catchments and between the hourly heavy rainfall and floods in small catchments, which is related to the travel times of water within the catchments.

hourly heavy rainfall has increased by 15%. In the south, floods have increased by about 20%, with hourly heavy rainfall increasing by 15% (Fig. 3b). After accounting for measurement errors in the heavy rainfall, correlations between the floods and heavy rainfall showed little change (Extended Data Table 2).

The close correspondence between floods and rainfall became apparent because of the availability of a very detailed, high-quality dataset of both heavy rainfall and floods. In the small catchments, floods have increased more than in the large catchments for two reasons. First, hourly heavy rainfall has increased more than daily heavy rainfall. The second reason relates to the more nonlinear behaviour of runoff generation processes in small catchments compared to those in larger catchments[5,48,49]. In small catchments, a 1% increase in heavy rain can translate into an increase in flood peak discharge of at least 2% (that is, an elasticity or amplification of more than 2% per %), whereas in large catchments, the elasticity tends to be smaller[5,48]. The stronger amplification in the north compared to the south (Fig. 3b) could be related to a more pronounced increase in soil moisture in the north, which tends to enhance flooding[5]. A comparison of flood magnitudes throughout the year, including winter events, with heavy rainfall gave a similarly close alignment, albeit the flood increases were smaller (Extended Data Fig. 8c,d).

An important finding is that daily rainfall changes are the main driver of flood changes in medium-sized and large catchments[5]. Observations from around the world have shown positive and negative flood trends, depending on the region[4,50–54]. In Austria, the flood trends in the north are much larger than those in the south (Fig. 3a). This lack of universality is entirely consistent with changes in the daily heavy rainfall and its drivers, and is also related to the role of other processes, such as snow melt, soil moisture variations and evaporation[55,56]. Consequently, there is little direct relationship between temperature increases and flood changes in medium-sized and large catchments.

For floods in small catchments (catchment areas <50 km^2), and for hourly rainfall, the observational database is globally much sparser. Our study shows that floods in small catchments in Austria have increased substantially, and the increases are closely aligned with increases in hourly heavy rainfall, based on the most comprehensive database from two independent networks. This close alignment can be explained by the short travel times of water in small catchments. North of the Alpine ridge, these increases are similar to those in the South. This is because of similar increases in the hourly heavy rainfall, which in turn are related to local convection processes that are, in the study region, apparently only weakly coupled with the dynamics of the atmospheric circulation and more associated with increases in the atmospheric energy content. This finding suggests that the increase in floods in small catchments may be more universal, not only applying to Austria, where long-time observations are available, but also to other parts of the world that are climatologically similar but where data are scarce. Because of the nonlinearity of the rainfall–runoff process[48], a given change in hourly heavy rainfall will translate into even bigger changes in floods in small catchments. With an elasticity of 2% per % of the rainfall–runoff process[17] (Fig. 3b) and an hourly rainfall scaling of 7% °C^{-1} (Fig. 2e), a regional 2 °C air temperature increase will translate into a 28% increase in flood discharge in small catchments. Further research is needed to assess the role of circulation changes, orographic processes and moisture sources.

Our study highlights that floods in small and large catchments can change in very different ways. This is because of the shorter water travel times in small catchments and thus the larger role of shorter-duration heavy rainfall, as well as differences in processes translating rainfall into runoff. Because of the closer tie of convective precipitation to energy availability, it seems that the increases in hourly heavy rainfall of 15% and the concomitant flood increases of 30% in small catchments can be generalized to other midlatitude catchments around the world where air temperature increases and moisture availability are similar. The implications for climate adaptation in flood risk management are major, with a need for emphasis on the differences between flood changes in small and large catchments. This is extremely important because of the manifold flood impacts in small catchments, including pluvial flooding in urban areas and landslides in steep landscapes. Also, many of the world's dams have catchment areas of only a few tenths of a square kilometre[57]. Because flood increases in small catchments seem to be larger and more universal than in large catchments, more consistent action is needed in the former.

Online content

Any methods, additional references, Nature Portfolio reporting summaries, source data, extended data, supplementary information, acknowledgements, peer review information; details of author contributions and competing interests; and statements of data and code availability are available at https://doi.org/10.1038/s41586-025-08647-2.

1. IPCC *Climate Change 2021: The Physical Science Basis* (eds Masson-Delmotte, V. et al.) (Cambridge Univ. Press, 2023).
2. Fowler, H. J. et al. Anthropogenic intensification of short-duration rainfall extremes. *Nat. Rev. Earth Environ.* **2**, 107–122 (2021).
3. Rajczak, J. & Schär, C. Projections of future precipitation extremes over Europe: a multimodel assessment of climate simulations: projections of precipitation extremes. *J. Geophys. Res. Atmos.* **122**, 10773–10800 (2017).
4. Merz, B. et al. Causes, impacts and patterns of disastrous river floods. *Nat. Rev. Earth Environ.* **2**, 592–609 (2021).
5. Blöschl, G. Three hypotheses on changing river flood hazards. *Hydrol. Earth Syst. Sci.* **26**, 5015–5033 (2022).
6. De Vries, I. E., Sippel, S., Pendergrass, A. G. & Knutti, R. Robust global detection of forced changes in mean and extreme precipitation despite observational disagreement on the magnitude of change. *Earth Syst. Dyn.* **14**, 81–100 (2023).
7. Zeder, J. & Fischer, E. M. Observed extreme precipitation trends and scaling in Central Europe. *Weather Clim. Extrem.* **29**, 100266 (2020).
8. Hofstätter, M., Lexer, A., Homann, M. & Blöschl, G. Large-scale heavy precipitation over Central Europe and the role of atmospheric cyclone track types. *Int. J. Climatol.* **38**, e497–e517 (2018).
9. Berg, P. & Haerter, J. O. Unexpected increase in precipitation intensity with temperature — a result of mixing of precipitation types? *Atmos. Res.* **119**, 56–61 (2013).
10. Formayer, H. & Fritz, A. Temperature dependency of hourly precipitation intensities – surface versus cloud layer temperature. *Int. J. Climatol.* **37**, 1–10 (2017).
11. Lenderink, G. & Van Meijgaard, E. Increase in hourly precipitation extremes beyond expectations from temperature changes. *Nat. Geosci.* **1**, 511–514 (2008).
12. Lenderink, G., Mok, H. Y., Lee, T. C. & Van Oldenborgh, G. J. Scaling and trends of hourly precipitation extremes in two different climate zones – Hong Kong and The Netherlands. *Hydrol. Earth Syst. Sci.* **15**, 3033–3041 (2011).
13. Lewis, E. et al. GSDR: a global sub-daily rainfall dataset. *J. Clim.* **32**, 4715–4729 (2019).
14. Lanza, L. G. & Vuerich, E. The WMO field intercomparison of rain intensity gauges. *Atmospheric Res.* **94**, 534–543 (2009).
15. Cauteruccio, A., Colli, M., Stagnaro, M., Lanza, L. G. & Vuerich, E. in *Springer Handbook of Atmospheric Measurements* (ed. Foken, T.) 359–400 (Springer, 2021).
16. Sivapalan, M., Blöschl, G., Merz, R. & Gutknecht, D. Linking flood frequency to long-term water balance: incorporating effects of seasonality. *Water Resour. Res.* **41**, 2004WR003439 (2005).
17. Breinl, K., Lun, D., Müller-Thomy, H. & Blöschl, G. Understanding the relationship between rainfall and flood probabilities through combined intensity–duration–frequency analysis. *J. Hydrol.* **602**, 126759 (2021).
18. Brunetti, M. et al. Precipitation variability and changes in the greater Alpine region over the 1800–2003 period. *J. Geophys. Res.* **111**, D11107 (2006).
19. Haslinger, K., Holawe, F. & Blöschl, G. Spatial characteristics of precipitation shortfalls in the greater Alpine region—a data-based analysis from observations. *Theor. Appl. Climatol.* **136**, 717–731 (2019).
20. Haslinger, K., Hofstätter, M., Schöner, W. & Blöschl, G. Changing summer precipitation variability in the Alpine region: on the role of scale dependent atmospheric drivers. *Clim. Dyn.* **57**, 1009–1021 (2021).
21. Bladé, I., Liebmann, B., Fortuny, D. & Van Oldenborgh, G. J. Observed and simulated impacts of the summer NAO in Europe: implications for projected drying in the Mediterranean region. *Clim. Dyn.* **39**, 709–727 (2012).
22. Ghosh, R., Müller, W. A., Baehr, J. & Bader, J. Impact of observed North Atlantic multidecadal variations to European summer climate: a linear baroclinic response to surface heating. *Clim. Dyn.* **48**, 3547–3563 (2017).
23. Awan, N. K. & Formayer, H. Cutoff low systems and their relevance to large-scale extreme precipitation in the European Alps. *Theor. Appl. Climatol.* **129**, 149–158 (2017).
24. van Bebber, W. *Die Zugstrassen der barometrischen Minima nach den Bahnenkarten der deutschen Seewarte für den Zeitraum 1875–1890* (1891).
25. Coumou, D., Di Capua, G., Vavrus, S., Wang, L. & Wang, S. The influence of Arctic amplification on mid-latitude summer circulation. *Nat. Commun.* **9**, 2959 (2018).
26. Coumou, D., Lehmann, J. & Beckmann, J. The weakening summer circulation in the Northern Hemisphere mid-latitudes. *Science* **348**, 324–327 (2015).
27. Francis, J. A., Skific, N. & Vavrus, S. J. Increased persistence of large-scale circulation regimes over Asia in the era of amplified Arctic warming, past and future. *Sci. Rep.* **10**, 14953 (2020).
28. Screen, J. A. & Simmonds, I. Exploring links between Arctic amplification and mid-latitude weather. *Geophys. Res. Lett.* **40**, 959–964 (2013).
29. Barnes, E. A. Revisiting the evidence linking Arctic amplification to extreme weather in midlatitudes. *Geophys. Res. Lett.* **40**, 4734–4739 (2013).
30. Kang, J. M., Shaw, T. A. & Sun, L. Arctic sea ice loss weakens Northern Hemisphere summertime storminess but not until the late 21st century. *Geophys. Res. Lett.* **50**, e2022GL102301 (2023).
31. Guilbert, J., Betts, A. K., Rizzo, D. M., Beckage, B. & Bomblies, A. Characterization of increased persistence and intensity of precipitation in the northeastern United States. *Geophys. Res. Lett.* **42**, 1888–1893 (2015).
32. Du, H. et al. Extreme precipitation on consecutive days occurs more often in a warming climate. *Bull. Am. Meteorol. Soc.* **103**, E1130–E1145 (2022).
33. Stjern, C. W. et al. The time scales of climate responses to carbon dioxide and aerosols. *J. Clim.* **36**, 3537–3551 (2023).
34. Sillmann, J. et al. Extreme wet and dry conditions affected differently by greenhouse gases and aerosols. *npj Clim. Atmos. Sci.* **2**, 24 (2019).
35. Risser, M. D. et al. Anthropogenic aerosols mask increases in US rainfall by greenhouse gases. *Nat. Commun.* **15**, 1318 (2024).
36. Berg, P., Moseley, C. & Haerter, J. O. Strong increase in convective precipitation in response to higher temperatures. *Nat. Geosci.* **6**, 181–185 (2013).
37. Park, I.-H. & Min, S.-K. Role of convective precipitation in the relationship between subdaily extreme precipitation and temperature. *J. Clim.* **30**, 9527–9537 (2017).
38. Duethmann, D. & Blöschl, G. Why has catchment evaporation increased in the past 40 years? A data-based study in Austria. *Hydrol. Earth Syst. Sci.* **22**, 5143–5158 (2018).
39. Vicente-Serrano, S. M. et al. Recent changes of relative humidity: regional connections with land and ocean processes. *Earth Syst. Dyn.* **9**, 915–937 (2018).
40. Schroeer, K. & Kirchengast, G. Sensitivity of extreme precipitation to temperature: the variability of scaling factors from a regional to local perspective. *Clim. Dyn.* **50**, 3981–3994 (2018).
41. Madsen, H., Arnbjerg-Nielsen, K. & Mikkelsen, P. S. Update of regional intensity–duration–frequency curves in Denmark: tendency towards increased storm intensities. *Atmos. Res.* **92**, 343–349 (2009).
42. Xiao, C., Wu, P., Zhang, L. & Song, L. Robust increase in extreme summer rainfall intensity during the past four decades observed in China. *Sci. Rep.* **6**, 38506 (2016).
43. Allan, R. P. et al. Advances in understanding large-scale responses of the water cycle to climate change. *Ann. N. Y. Acad. Sci.* **1472**, 49–75 (2020).
44. Ali, H. et al. Towards quantifying the uncertainty in estimating observed scaling rates. *Geophys. Res. Lett.* **49**, e2022GL099138 (2022).
45. Formetta, G., Marra, F., Dallan, E., Zaramella, M. & Borga, M. Differential orographic impact on sub-hourly, hourly, and daily extreme precipitation. *Adv. Water Resour.* **159**, 104085 (2022).
46. Marra, F., Armon, M., Borga, M. & Morin, E. Orographic effect on extreme precipitation statistics peaks at hourly time scales. *Geophys. Res. Lett.* **48**, e2020GL091498 (2021).
47. Chan, S. C., Kendon, E. J., Roberts, N. M., Fowler, H. J. & Blenkinsop, S. Downturn in scaling of UK extreme rainfall with temperature for future hottest days. *Nat. Geosci.* **9**, 24–28 (2016).
48. Blöschl, G. Flood generation: process patterns from the raindrop to the ocean. *Hydrol. Earth Syst. Sci.* **26**, 2469–2480 (2022).
49. Brunner, M. I. et al. An extremeness threshold determines the regional response of floods to changes in rainfall extremes. *Commun. Earth Environ.* **2**, 173 (2021).
50. Hall, J. et al. Understanding flood regime changes in Europe: a state-of-the-art assessment. *Hydrol. Earth Syst. Sci.* **18**, 2735–2772 (2014).
51. Archfield, S. A., Hirsch, R. M., Viglione, A. & Blöschl, G. Fragmented patterns of flood change across the United States. *Geophys. Res. Lett.* **43**, 10232–10239 (2016).
52. Blöschl, G. et al. Changing climate both increases and decreases European river floods. *Nature* **573**, 108–111 (2019).
53. Yang, L. et al. Climate more important for Chinese flood changes than reservoirs and land use. *Geophys. Res. Lett.* **48**, e2021GL093061 (2021).
54. Chagas, V. B. P., Chaffe, P. L. B. & Blöschl, G. Climate and land management accelerate the Brazilian water cycle. *Nat. Commun.* **13**, 5136 (2022).
55. Bertola, M., Viglione, A., Lun, D., Hall, J. & Blöschl, G. Flood trends in Europe: are changes in small and big floods different? *Hydrol. Earth Syst. Sci.* **24**, 1805–1822 (2020).
56. Bertola, M. et al. Do small and large floods have the same drivers of change? A regional attribution analysis in Europe. *Hydrol. Earth Syst. Sci.* **25**, 1347–1364 (2021).
57. International Commission on large dams. *World Register of Dams General Synthesis* www.icold-cigb.org/GB/world_register/general_synthesis.asp (2024).
58. Lun, D., Fischer, S., Viglione, A. & Blöschl, G. Significance testing of rank cross-correlations between autocorrelated time series with short-range dependence. *J. Appl. Stat.* **50**, 2934–2950 (2023).

Methods

Rainfall data

We used rain gauge data from two completely independent network operators: (1) GeoSphere Austria (GSA), the Federal Geological, Geophysical, Climatological and Meteorological Service of Austria (formerly known as Zentralanstalt für Meteorologie und Geodynamik), which operates nearly 300 rain gauge stations across Austria; and (2) the Federal Ministry of Agriculture, Forestry, Regions and Water Management, Directorate I/3, Water Balance (Hydrological Service, abbreviated HYD, which operates more than 1,000 rain gauge stations. In a trade-off between temporal coverage, spatial consistency and number of stations, a temporal coverage of 1948–2023 for daily GSA data, 1900–2023 for daily HYD data and 1950–2023 for hourly data was chosen. Based on the criteria of minimum data availability (see 'Statistical analysis of rainfall data' below), 63 daily GSA stations, 50 hourly GSA stations, 779 daily HYD stations and 163 hourly HYD stations were selected, totalling 883 stations due to some overlap between the hourly and daily stations. All records were quality checked and the daily GSA records were also homogenized[59,60].

The recording rain gauges of the GSA network were mainly floater devices before the 1980s. These were gradually replaced by PAAR AP23 tipping buckets with a 500-cm^2 collection area (10-s sampling frequency, 0.1-mm resolution, ±1% accuracy, per the manufacturer). After 2000, some stations were changed to total rain weighing system (TRWS)-MPS weighing gauges with a 500-cm^2 collection area (1-min sampling frequency, 0.06-mm h^{-1} resolution, 0.01-mm (depth) and 0.01-mm min^{-1} (intensity) resolution, per the manufacturer). The recording rain gauges of the HYD network consist mainly of over-the-top (OTT) Pluvio2 and Sommer Niwa-505 weighing gauges with collection areas of 200, 400 or 500 cm^2. There are fewer tipping buckets (mostly Sommer MR3), with 500-cm^2 collection areas (1-s sampling frequency, 0.1-mm accuracy, per the manufacturer) and optical sensors (mostly OTT Parsivel2). Before the 1980s, the recording rain gauges were typically taken out of operation during the colder months of the year (October–April), resulting in data gaps. Additionally, manual rain gauges (that is, ombrometers) were in operation. Extended Data Fig. 3 shows the evolution of the number of stations of each type over the study period and Table 1 gives the station years for each registration system.

Error correction of rainfall data due to registration type

Measurements of heavy rainfall are affected by errors due to wind drift and the registration system. Because the registration system changed during the observation period, it was essential to account for the latter type of error in the change analyses. Error characteristics from different automated rain gauges have been extensively evaluated in numerous field and laboratory experiments, and they differ between registration type[61,62]. We assessed plausible errors for each registration type as described in the following (Table 2). For the ombrometer, we chose ±0% because these were manual measurements where observers were typically aware of any observation errors. Although no literature was available for the floaters, anecdotal evidence from the network operators suggested frequent issues with the siphons of this system, so a relatively large error of −5% (underestimation) was chosen. For the tipping bucket type, a World Meteorological Organization (WMO) study[62] (Annex AP23 PAAR, laboratory test sheet graphic and field calibration sheet table) gave an error of −3% for a typical heavy rainfall intensity in the study area of 50–80 mm h^{-1}, and a slightly smaller error of −2.5% was assumed for daily rainfall. For the weighing gauge type, the WMO study[62] (Annex PLUVIO OTT and TRWS-MPS, laboratory test sheet graphic and field calibration sheet table) gave an error of −1% (TRWS-MPS) and ±0% (PLUVIO OTT) for the same intensity. Here we chose an error of −1% for all weighing gauges, and a slightly smaller error of −0.5% was assumed for daily rainfall. For the optical sensor type, the WMO study[62] (Annex PARSIVEL OTT, field intercomparison measurements sheet, upper panel graphic) gave an error of +20% for the same intensity—that is, a massive overestimation.

Statistical analysis of rainfall data

The heavy rainfall analysis focused on the warm season (May to September) because the floater gauges were not operated during the cold season. Given that heavy rainfall in the warm season was much higher than in the cold season[16,17], the results are also representative of the entire year. Heavy rainfall was defined as the 99th percentile of the rainfall time series of wet days (more than 0.2 mm d^{-1} of precipitation) and wet hours (more than 0.2 mm h^{-1} of precipitation). The 99th percentile was estimated within a 21-year moving window for robustness and plotted on the centre year. At the beginning and end of the series, the windows were allowed to be shorter, with a minimum of 11 years (first year and the following 10 years, last year and the preceding 10 years). A sensitivity analysis indicated that modifying the window size changed the evolution of the heavy rainfall only slightly. To the minimize the effect of missing data, we estimate the percentiles only for those moving windows for which a threshold of 50% of missing data was never exceeded in any month within the window, which resulted in a median number of estimated percentiles per rain gauge of 36 and 72 for the hourly and daily time series, respectively. Additionally, stations with fewer than 20 valid percentile estimates within the reference period 1981–2010 were excluded, resulting in 883 stations. Heavy rainfall anomalies were calculated by the difference in the percentiles from the moving windows and the average of these percentiles within the reference period, divided by that average for each station. A sensitivity analysis conducted by randomly subsampling the stations in the study area suggested little effect of station density on heavy rainfall anomalies (Extended Data Fig. 4). To quantify the co-occurrence of daily and hourly heavy rainfall, we calculated the fraction of days where the 99th percentile was exceeded in the reference period 1981–2010 on daily and hourly time scales for stations where both series were available. There was very little co-occurrence (on average, 9.0 ± 0.4% of the days).

We spatially stratified the heavy rainfall anomalies in two ways. The first stratification was into stations north and south of 47.6° N, representing the climate regimes of heavy rainfall north and south of the European Alps.

While the general climate divide coincides with the main Alpine ridge (47° N in Austria)[18,19], the dividing line for the heavy rainfall during summer was slightly farther north[8,23,63]. The second stratification was by altitude, with the stations grouped into lowland (less than or equal to 800 m above sea level (a.s.l.)) and mountain (more than 800 m a.s.l.) stations.

Temperature data

We used daily air temperature records from 63 stations in Austria, from the GSA and HYD networks, for instantaneous scaling of the heavy rainfall with air temperature changes. We used monthly air temperature records from 66 stations in Austria, from the Historical Instrumental Climatological Surface Time Series of the Greater Alpine Region (HISTALP) database[59], which were quality checked, outlier corrected and homogenized. For each year, the warm season (May to September) averages were normalized by their means over the reference period (1981–2010), separately for each station, which were then averaged over the entire study domain to obtain an annual time series of air temperature anomaly over the study domain. This time series was used for both climate scaling the heavy rainfall with air temperature changes and for the correlation analysis between heavy rainfall and air temperature.

Scaling analysis

The instantaneous scaling was based on quantile regression, estimating a linear relationship between the logarithm of the 99th percentile of the hourly and daily rainfall (dependent variables) and air

temperature (independent variable), pooling all stations, years and months. Quantile regression is more robust against outliers than more-common regression models on binned temperatures[40,64,65]. Uncertainty was assessed via bootstrapping of the coefficients of the quantile regression model (numbers in Fig. 2d and Extended Data Table 3). For visualization, the heavy rainfall was binned by month (lines in Fig. 2d). For the climate scaling, the spatial averages over all stations of heavy rainfall anomalies were averaged over two 21-year sub-periods (1950–1970 and 2003–2023), and the anomaly differences were evaluated for the hourly and daily heavy rainfall. A similar difference was calculated for the HISTALP air temperatures. The ratio between the two represented the climate scaling[66,67] (numbers in Fig. 2e and Extended Data Table 3). The uncertainty was estimated by bootstrapping.

Atmospheric circulation indices

Two indices of the atmospheric flow conditions (meridionality and persistency) over Central Europe were used in this study[20], which were based on a daily circulation type classification[68,69]. The circulation type classification has seven divisions, three (northeast, indifferent; east, indifferent; north cyclonic) considered meridional types because they exhibit a strong northerly flow component with low-pressure gradients across the domain[70], and two (west–southwest, cyclonic, flat pressure; westerly flow over Northern Europe) considered zonal types because they exhibit strong westerly flow components and pronounced pressure gradients. The remaining two denote pure cyclonic/anticyclonic circulation types.

The meridionality index is the difference between the frequencies of the meridional and zonal circulation types in the summer of the respective year, scaled by their averages over the period 1900–2023. For comparability, the index was adjusted to a zero mean over the reference period 1981–2010. A positive meridionality index indicates the dominance of meridional flow in the reference period. For each of the seven circulation types, the probability that the circulation type of any one day was the same as that of the previous day was calculated. The persistency index is the average of these probabilities of the seven circulation types for each year[71,72], adjusted to a unit variance and zero mean over the reference period. A positive persistency index indicates stronger persistence than the average of the reference period. The same 21-year moving averaging window as for heavy rainfall was applied to both the meridionality and persistency index to highlight the long-term fluctuations.

Cyclone track indices

Additional information included the tracks of cyclones moving across Europe, based on schemes for detecting[73] and classifying[63] cyclones by their origin and paths (6-h time step) over the time period 1960–2017. We singled out two track groups—Vb and X-N, representing heavy rainfall in northern Austria, and X-S, representing heavy rainfall in southern Austria[8]. The first cyclone track index was the frequency of Vb and X-N tracks in each year standardized by its mean over the reference period 1981–2010 and scaled to unit variance, with the second being the equivalent index for the X-S tracks. A 21-year moving averaging window was applied to both indices.

Aerosol data

To explore other effects on the heavy rainfall, we use two datasets of sulfate aerosol concentrations. The first were sub-annually resolved reconstructions from the ice cores of the Colle Gnifetti ice cap in the Italian Alps[74], the second were annually resolved reconstructions from the winter snowpack on a glacier field near the Sonnblick Observatory in the Austrian Alps[75].

Flood peak data and analysis

The flood data were obtained from the pan-European Flood Database[52,76,77]. The dataset consists of the highest discharge (daily mean or instantaneous discharge) in each calendar year from 8,023 river gauges in Europe. Here we used flood data from 693 catchments with centroids within Austria, or no more than 30 km outside Austria, with at least 10 years' worth of data in the reference period 1981–2010. The catchments ranged in size from 1 to 250,000 km^2.

Flood anomalies were calculated by dividing the annual maximum discharges of each series by their average over the reference period 1981–2010, from which unity was subtracted. The flood anomalies were then smoothed using a centred moving averaging window of 41 years. We chose a longer window than the 21-year window for the heavy rainfall because the temporal fluctuations of the floods were larger and the aim was to represent the decadal scale changes in a comparable way. In Extended Data Fig. 8, we used the maximum flood peaks for the entire year, whereas in Fig. 3, we used the maximum flood peaks from the warm season, again for comparability with the heavy rainfall. Across the study region, most of the maximum annual discharges in summer were caused by rainfall, with snow melt accounting for only 5% of the summer events (Merz and Blöschl, 2003). In relating flood discharges to heavy rainfall, we introduced a classification into catchments smaller than 50 km^2 and larger than 500 km^2. A sensitivity analysis suggested that the temporal flood–rainfall correlations were only a little sensitive to the choice of catchment size threshold.

Correlation analysis

We use Spearman's rank correlation analysis to estimate the strength of the relationship between the heavy rainfall anomalies and their potential drivers (meridionality index, persistency index, air temperature) and between the heavy rainfall and floods. We chose Spearman correlations because not all the relationships were expected to be linear. In estimating the significance of the correlations, we accounted for the autocorrelation of the anomalies, exacerbated by the moving averaging window, by a recently developed method[58].

Data availability

All data for conducting the analysis, including raw station data and external data, are available at Zenodo (https://doi.org/10.5281/zenodo.12684482)[78]. External data is available at the Zenodo archive and via the following resources: monthly air temperature data: https://www.zamg.ac.at/histalp; aerosol data (Colle Gniffetti ice cap): https://doi.pangaea.de/10.1594/PANGAEA.894788.

Code availability

All code for conducting the analysis is available at Zenodo (https://doi.org/10.5281/zenodo.12684482)[78].

59. Auer, I. et al. HISTALP—historical instrumental climatological surface time series of the greater Alpine region. *Int. J. Climatol.* **27**, 17–46 (2007).
60. Nemec, J., Gruber, C., Chimani, B. & Auer, I. Trends in extreme temperature indices in Austria based on a new homogenised dataset. *Int. J. Climatol.* **33**, 1538–1550 (2013).
61. Lanza, L., Leroy, M., Alexandropoulos, C., Stagi, L. & Wauben, W. *The WMO Laboratory Intercomparison of Rainfall Intensity Gauges: Final Report*. Instruments and Observing Methods Report No. 84 (World Meteorological Organization, 2006).
62. World Meteorological Organization (WMO). *WMO Field Intercomparison of Rainfall Intensity Gauges*. 290 (2009).
63. Hofstätter, M., Chimani, B., Lexer, A. & Blöschl, G. A new classification scheme of European cyclone tracks with relevance to precipitation. *Water Resour. Res.* **52**, 7086–7104 (2016).
64. Wasko, C., Sharma, A. & Johnson, F. Does storm duration modulate the extreme precipitation-temperature scaling relationship? *Geophys. Res. Lett.* **42**, 8783–8790 (2015).
65. Westra, S. et al. Future changes to the intensity and frequency of short-duration extreme rainfall. *Rev. Geophys.* **52**, 522–555 (2014).
66. Bao, J., Sherwood, S. C., Alexander, L. V. & Evans, J. P. Future increases in extreme precipitation exceed observed scaling rates. *Nat. Clim. Change* **7**, 128–132 (2017).
67. Zhang, S., Stier, P., Dagan, G., Zhou, C. & Wang, M. Sea surface warming patterns drive hydrological sensitivity uncertainties. *Nat. Clim. Change* **13**, 545–553 (2023).
68. Schwander, M. et al. Reconstruction of Central European daily weather types back to 1763. *Int. J. Climatol.* **37**, 30–44 (2017).

69. Pfister, L., Wilhelm, L., Brugnara, Y., Imfeld, N. & Brönnimann, S. Weather type reconstruction using machine learning approaches. Preprint at *EGUsphere* https://doi.org/10.5194/egusphere-2024-1346 (2024).
70. Haslinger, K. et al. Disentangling drivers of meteorological droughts in the European greater Alpine region during the last two centuries. *J. Geophys. Res. Atmos.* **124**, 12404–12425 (2019).
71. Richardson, D., Kilsby, C. G., Fowler, H. J. & Bárdossy, A. Weekly to multi-month persistence in sets of daily weather patterns over Europe and the North Atlantic Ocean. *Int. J. Climatol.* **39**, 2041–2056 (2019).
72. Jordan, P. & Talkner, P. A seasonal Markov chain model for the weather in the Central Alps. *Tellus Dyn. Meteorol. Oceanogr.* **52**, 455–469 (2000).
73. Wernli, H. & Schwierz, C. Surface cyclones in the ERA-40 dataset (1958–2001). Part I: novel identification method and global climatology. *J. Atmos. Sci.* **63**, 2486–2507 (2006).
74. Sigl, M. et al. 19th century glacier retreat in the Alps preceded the emergence of industrial black carbon deposition on high-alpine glaciers. *Cryosphere* **12**, 3311–3331 (2018).
75. Greilinger, M., Schöner, W., Winiwarter, W. & Kasper-Giebl, A. Temporal changes of inorganic ion deposition in the seasonal snow cover for the Austrian Alps (1983–2014). *Atmos. Environ.* **132**, 141–152 (2016).
76. Blöschl, G. et al. Changing climate shifts timing of European floods. *Science* **357**, 588–590 (2017).
77. Bertola, M. et al. Megafloods in Europe can be anticipated from observations in hydrologically similar catchments. *Nat. Geosci.* **16**, 982–988 (2023).
78. Haslinger, K. et al. Data and code for 'Increasing hourly heavy rainfall in Austria reflected in flood changes'. *Zenodo* https://doi.org/10.5281/zenodo.12684482 (2025).

Acknowledgements This work was supported by the European Research Council (ERC) Advanced Grant FloodChange project (no. 291152), the Austrian Science Funds SPATE project (number I4776) and the Interreg Alpine Space project X-RISK-CC (no. ASP0100101). We thank R. Potzmann for discussions on rain gauge errors.

Author contributions K.H. and G.B. designed the study and wrote the first draft of the paper. K.H., L.P., M.B. and M.G. collated the database, K.H., K.B., L.P. and M.B. conducted the statistical analysis. K.H., K.B., L.P., G.P., M.B., M.O., M.G., W.S. and G.B. interpreted the results and contributed to revising the paper.

Competing interests The authors declare no competing interests.

Additional information
Correspondence and requests for materials should be addressed to Klaus Haslinger.
Peer review information *Nature* thanks Yang Chen, Benjamin Poschlod and the other, anonymous, reviewer(s) for their contribution to the peer review of this work.

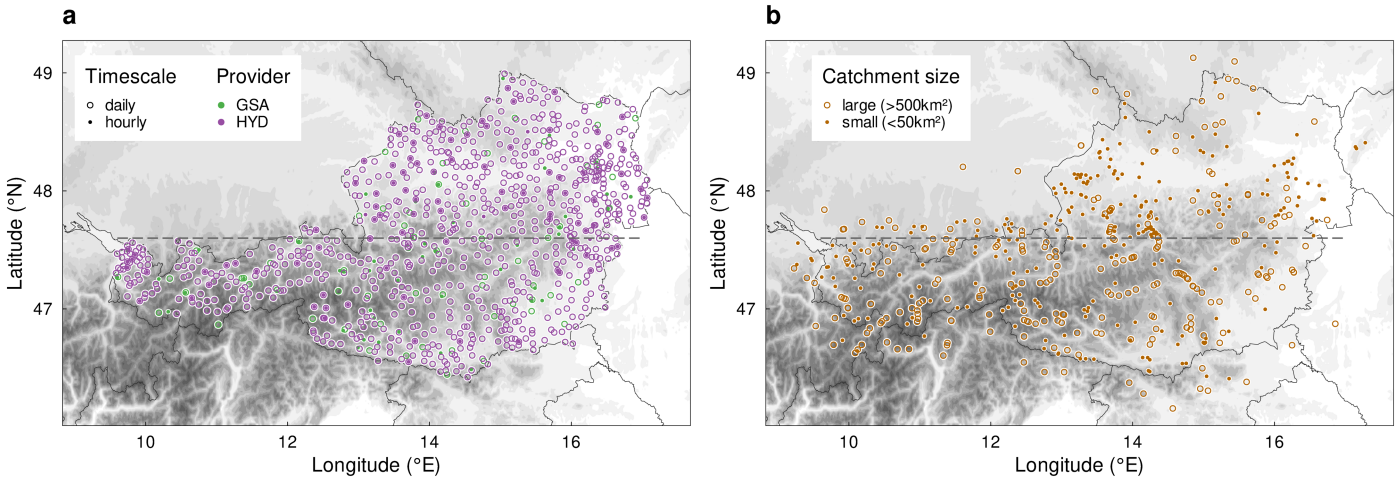

Extended Data Fig. 1 | Location of the rain gauges and catchments. **a**, Location of the rain gauges, circles indicate daily gauges, dots hourly gauges. Colours indicate the data provider (green: GSA, purple: HYD). **b**, Location of the catchment centroids; circles indicate large catchments (>500 km²), dots small catchments (<50 km²). Dashed line indicates the North/South divide of the region at 47.6°N.

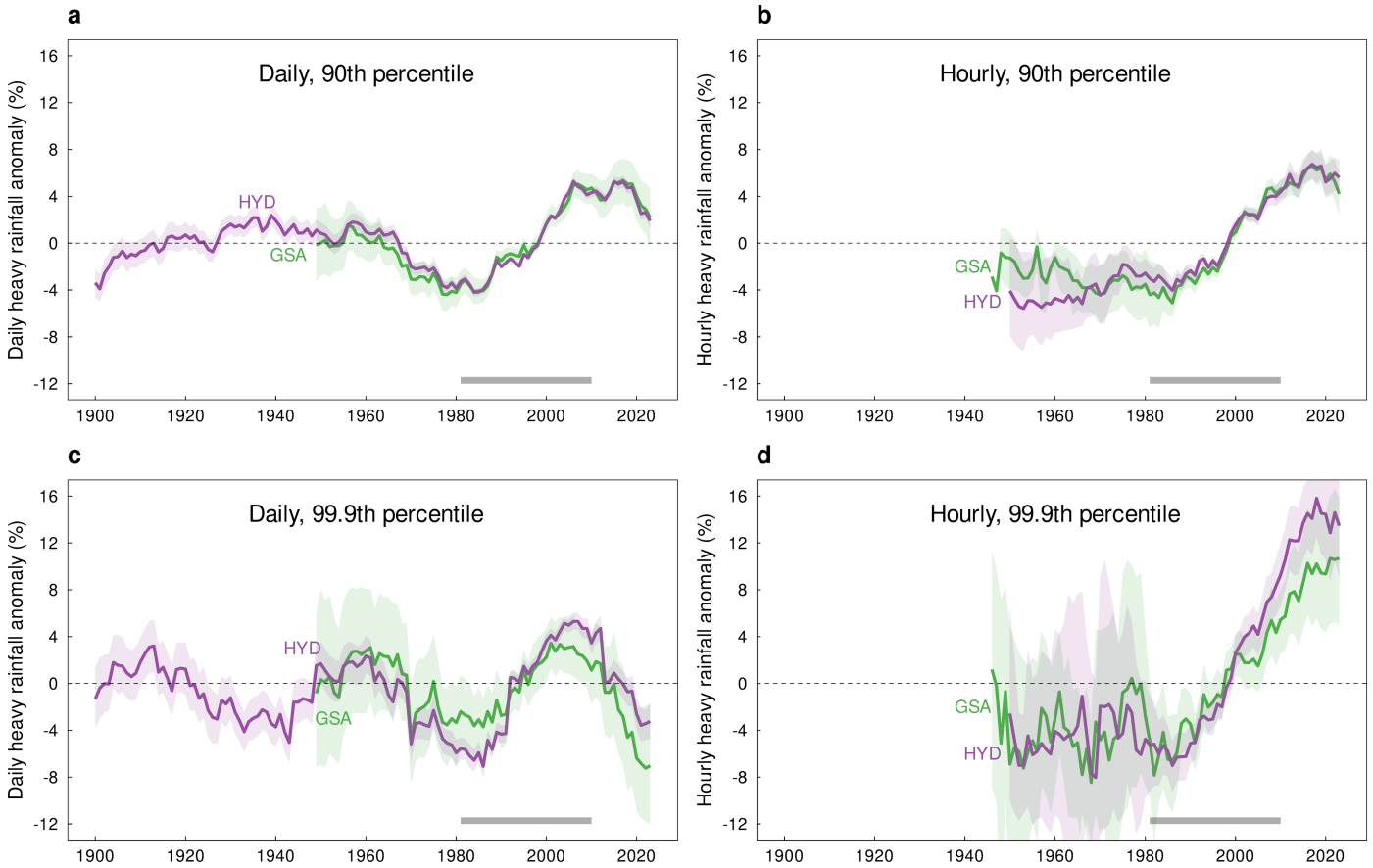

Extended Data Fig. 2 | Heavy rainfall evolution in Austria based on the 90th and 99.9th percentile. a, Daily heavy rainfall (90th percentiles of wet days) anomalies with respect to the reference period 1981–2010 calculated from the GSA (green) and HYD (purple) datasets. Solid lines indicate the mean over all stations, shaded bands the 95% confidence interval of the mean estimated by bootstrapping (n = 1000). The confidence intervals of the GSA data are wider because of the smaller number of stations. **b**, Hourly heavy rainfall (90th percentiles of wet hours) anomalies similar to a. **c** and **d**, as in a and b but for the 99.9th percentile. The grey bars at the bottom of the panels indicate the reference period. The heavy rainfall evolution of the 90th and 99.9th percentiles is similar to the 99th percentiles in Fig. 1.

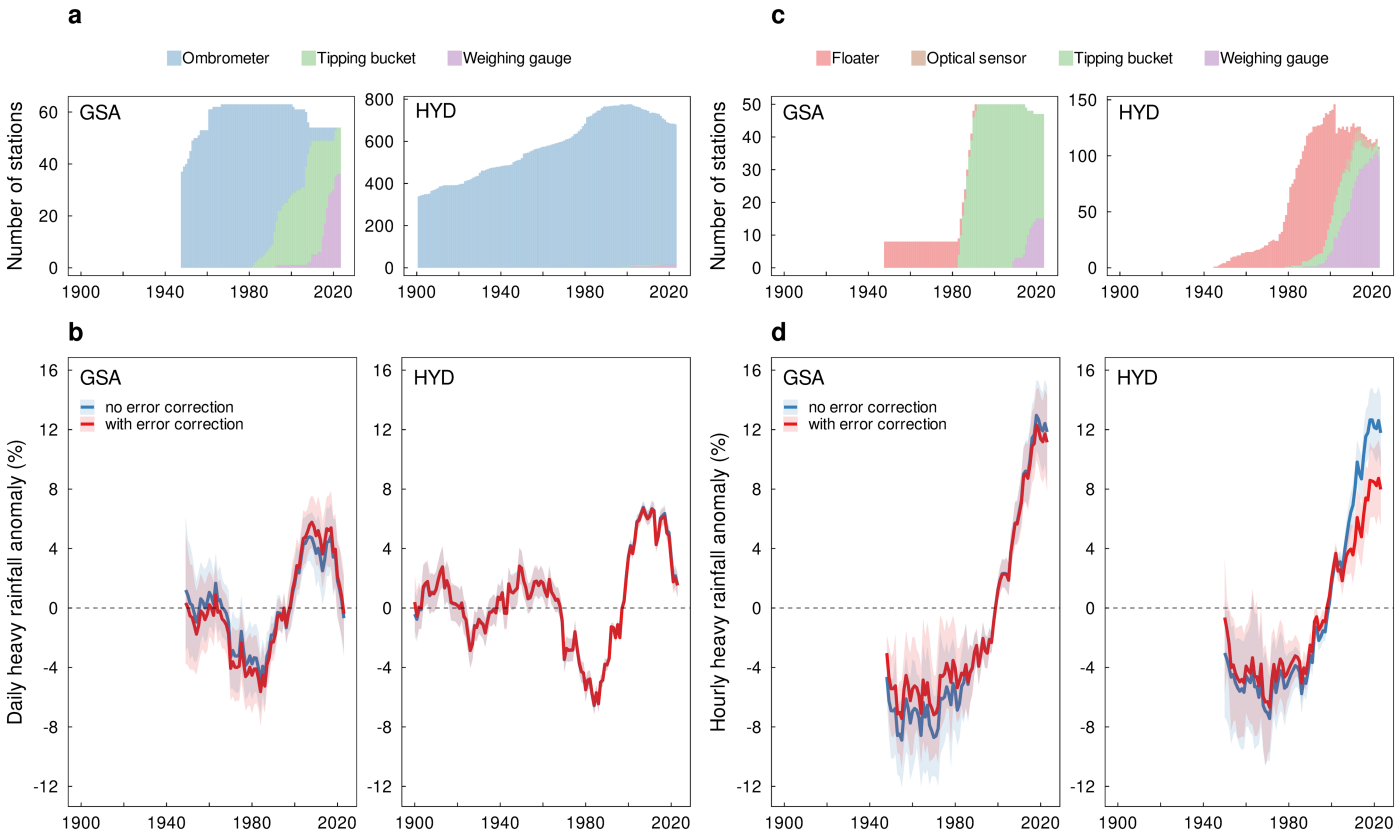

Extended Data Fig. 3 | Heavy rainfall evolution in Austria and the effect of measurement error correction. a, Registration types of the GSA and HYD rain gauges for daily rainfall totals over time. **b**, Daily heavy rainfall anomalies with respect to the reference period 1981–2010 for the GSA (left) and HYD (right) datasets, without (blue) and with (red) correction of the errors caused by the registration type. Solid lines indicate the mean over all stations, shaded bands the 95% confidence interval of the mean estimated by bootstrapping (n = 1000). **c**, As in a but for hourly data. **d**, As in b but for hourly data. Error correction as per Table 2.

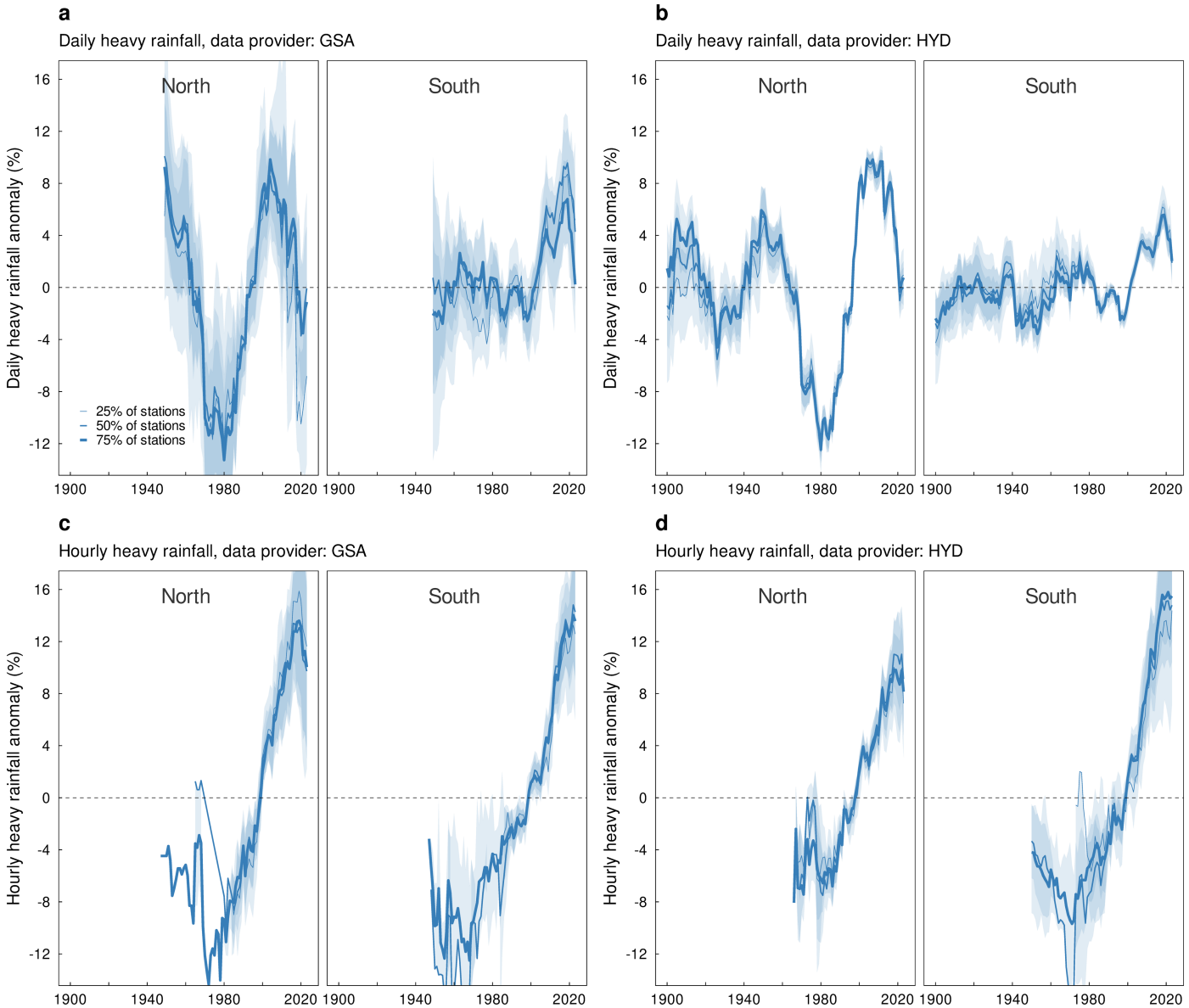

Extended Data Fig. 4 | Effect of number of stations (25, 50 and 75% of the stations available) on heavy rainfall anomalies. a, Daily heavy rainfall (99th percentiles of wet days) anomalies with respect to the reference period 1981–2010 calculated from the GSA data for the North and South. **b**, As for **a** but for the HYD data. **c**, **d**, As for **a**,**b**, but for hourly data. Solid lines indicate the mean over all stations, shaded bands the 95% confidence interval of the mean estimated by bootstrapping (n = 1000). There is little effect of station density on the estimated heavy rainfall evolution.

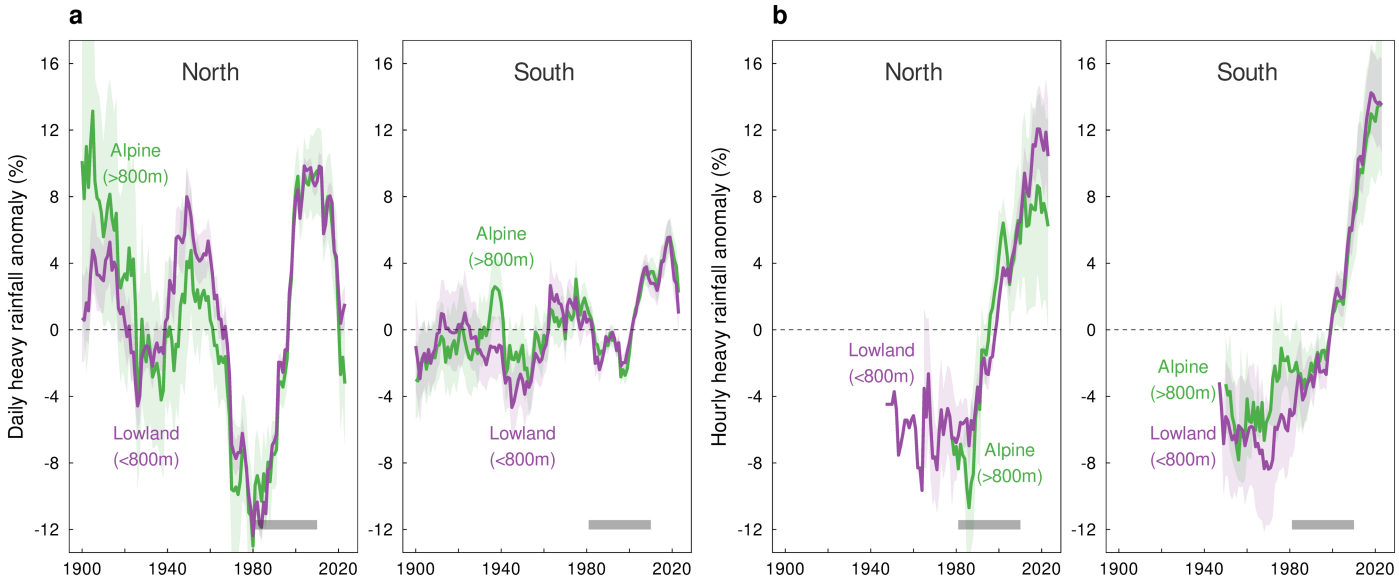

Extended Data Fig. 5 | Heavy rainfall evolution in Austria, stratified by altitude. a, Daily heavy rainfall (99th percentiles of wet days) anomalies with respect to the reference period 1981–2010 for stations higher than 800 m elevation (green) and lower than 800 m elevation (purple), north (left) and south (right) of the Alpine ridge. Both data sets, i.e. GSA and HYD merged. Solid lines indicate the mean over all stations, shaded bands the 95% confidence interval of the mean estimated by bootstrapping (n = 1000). **b**, As in **a** but for hourly data. The grey bars at the bottom of each panel indicate the reference period. There is little effect of elevation on heavy rainfall evolution.

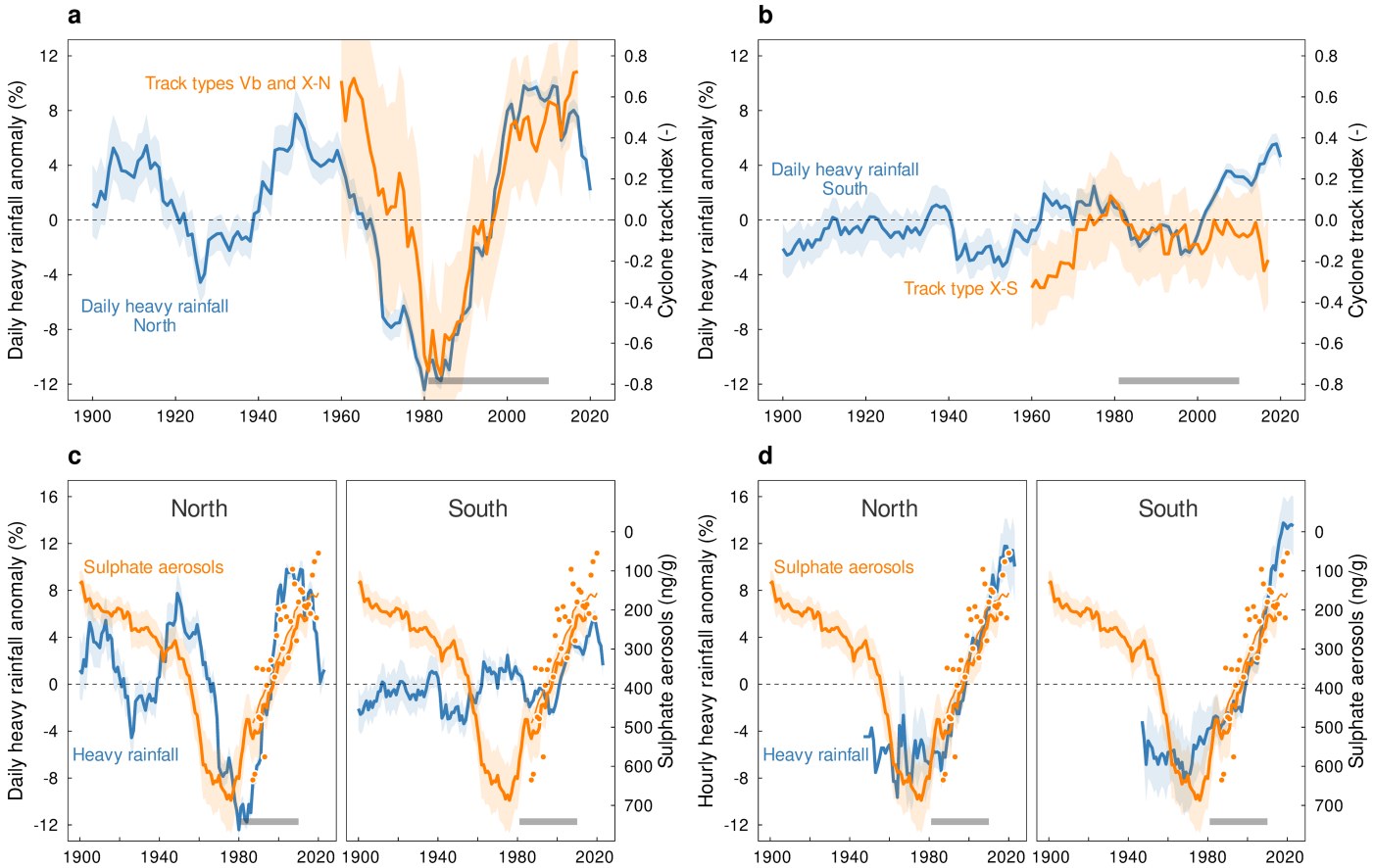

Extended Data Fig. 6 | Heavy rainfall evolution in Austria compared to sulphate aerosols and cyclone tracks. a, Daily heavy rainfall anomalies in the North, and Vb and X-N Cyclone track index. **b**, Daily heavy rainfall anomalies in the South, and X-S Cyclone track index. **c**, Daily heavy rainfall anomalies north (left) and south (right) of the Alpine ridge and sulphate aerosol concentrations from Colle Gnifetti, Italy (orange line) and Hoher Sonnblick, Austria (orange dots). y-axis of sulphate aerosols is inverted. **d**, Hourly heavy rainfall anomalies north (left) and south (right) of the Alpine ridge and sulphate aerosol concentrations as in **c**. Solid lines indicate the mean over all stations, shaded bands the 95% confidence interval of the mean estimated by bootstrapping (n = 1000). The grey bars at the bottom of the panels indicate the reference period.

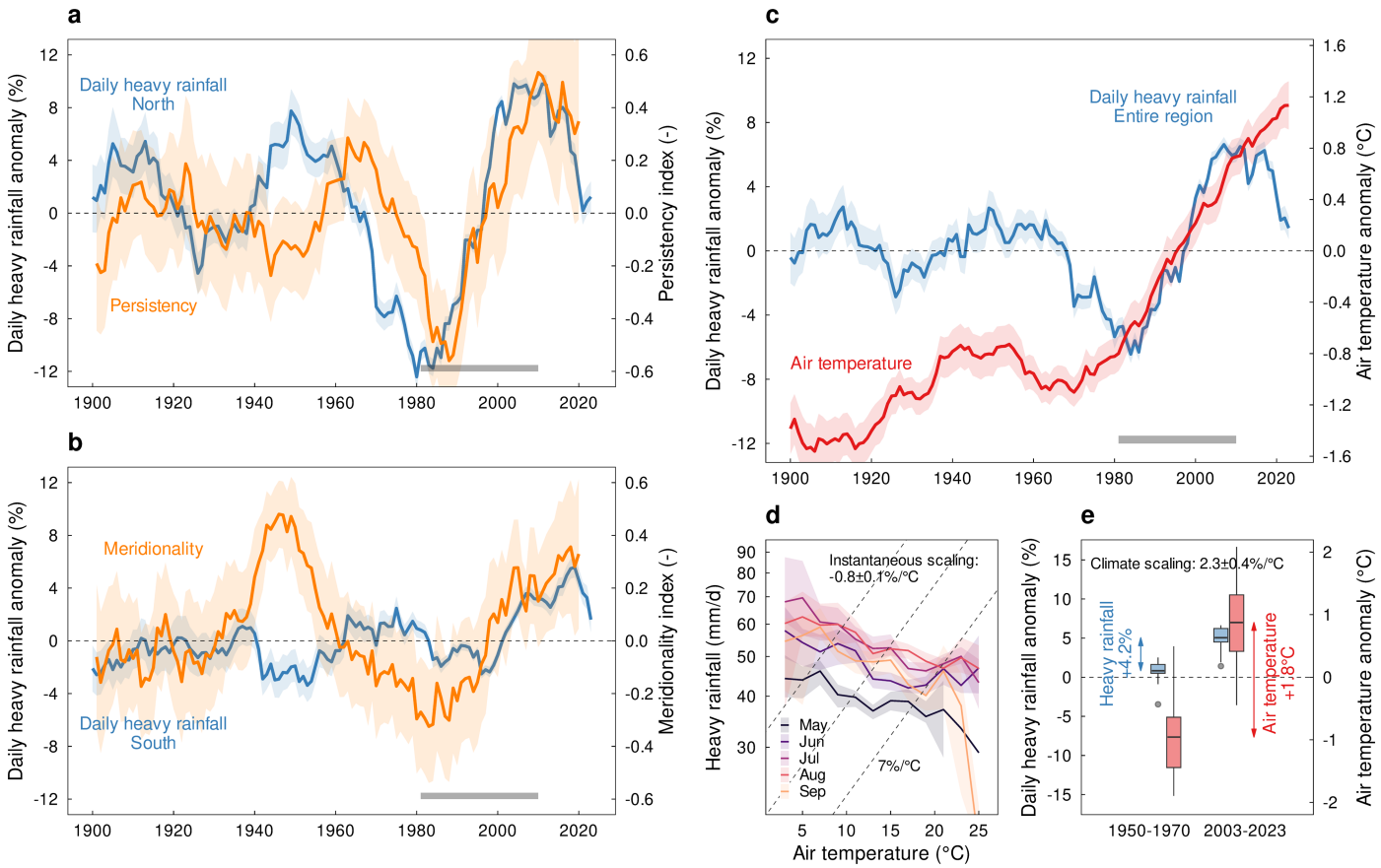

Extended Data Fig. 7 | Attribution of heavy rainfall evolution in Austria and temperature scaling with daily data. a, Daily heavy rainfall anomalies in the North and persistency index. **b**, Daily heavy rainfall anomalies in the South and meridionality index. **c**, Daily heavy rainfall anomalies and air temperature anomalies over the entire domain. **d**, *Instantaneous scaling*: daily heavy rainfall rates above the 99th percentile binned by daily air temperature of the day of occurrence for each month of the warm season. Grey dashed lines indicate scaling of +7%/°C. A quantile regression of (log-)hourly heavy rainfall against daily air temperature during 1950–2023 gives an instantaneous scaling across all months of −0.8 ± 0.1%/°C. **e**, *Climate scaling*: comparison of the periods 1950–1970 and 2003–2023. Average daily heavy rainfall anomaly increases by +4.2%, air temperature anomaly by +1.8 °C, which gives a climate scaling of 2.3 ± 0.4%/°C. The grey bars at the bottom of a, b and c indicate the reference period. Solid lines indicate the mean over all stations, shaded bands the 95% confidence interval of the mean estimated by bootstrapping (n = 1000). Lower and upper box boundaries in e are 25th and 75th percentiles, respectively, the line inside the box is the mean, the upper and lower whiskers extend to the largest value but no further than 1.5 times the interquartile range, and the points outside the whiskers are individual data points.

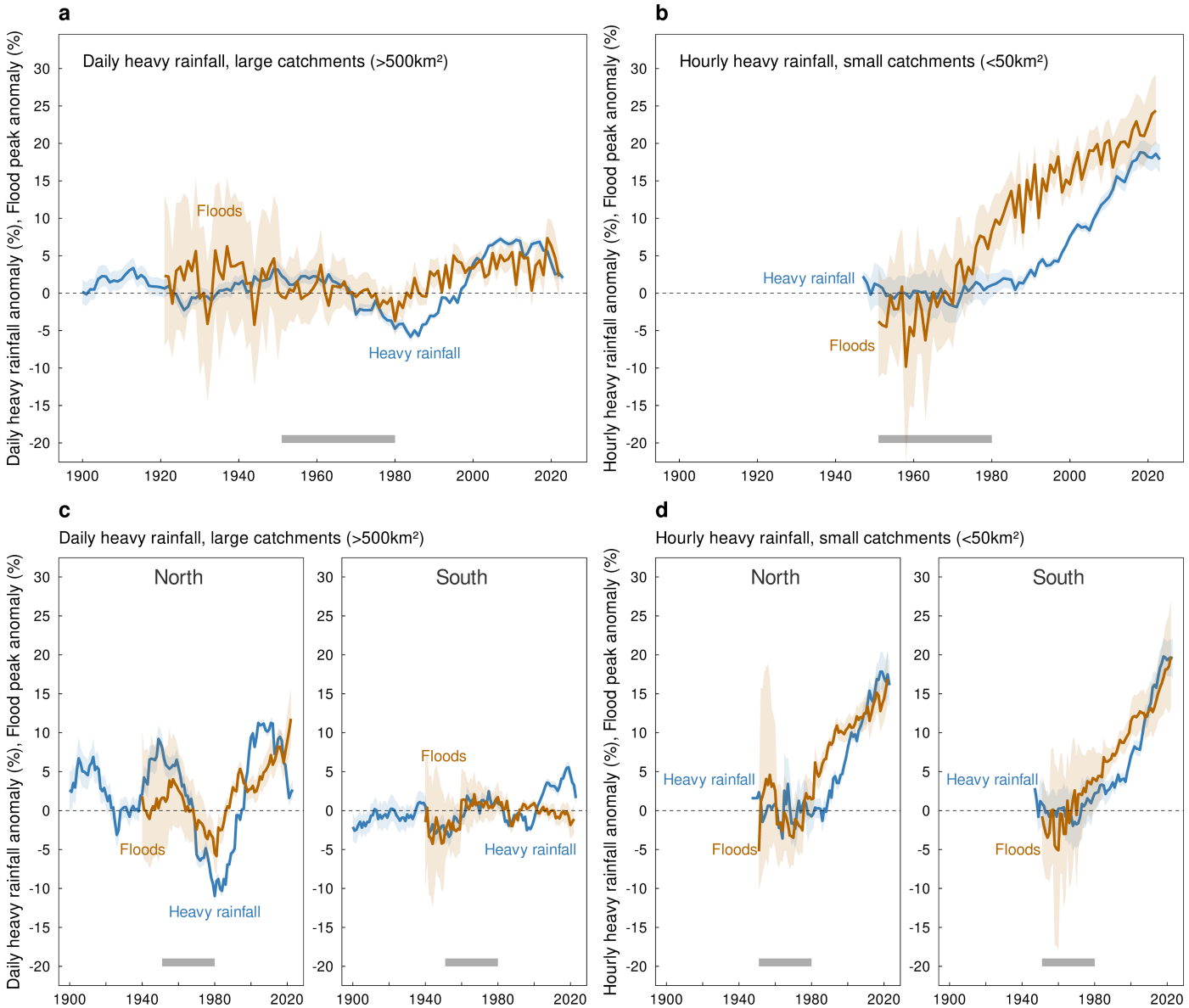

Extended Data Fig. 8 | Effect of heavy rainfall evolution on flood peaks considering either all of Austria or all the seasons. a, Daily heavy rainfall anomalies and flood peak discharge anomalies in the warm season for large catchments (>500 km²) in the entire domain. **b**, Hourly heavy rainfall anomalies and flood peak discharge anomalies the warm season for small catchments (<50 km²) in the entire domain. Heavy rainfall values are 99th percentiles as in Fig. 1, flood peaks are the mean annual floods of the warm season. **c**, Daily heavy rainfall anomalies and flood peak discharge anomalies in the entire year for large catchments (>500 km²), north (left) and south (right) of the Alpine ridge. **d**, Hourly heavy rainfall anomalies and flood peak discharge anomalies in the entire year for small catchments (<50 km²), north (left) and south (right) of the Alpine ridge. Solid lines indicate the mean over all stations, shaded bands the 95% confidence interval of the mean estimated by bootstrapping (n = 1000). The grey bars at the bottom of the panels indicate the reference period. The figure is similar to Fig. 3, but **a**,**b** show the anomalies for the entire domain rather than for the subregions north and south of the Alpine ridge, and **c**,**d** shows the all-year flood peak anomalies rather than the warm season.

Extended Data Table 1 | Spearman's rank correlation coefficients of daily and hourly heavy rainfall with meridionality index, persistency index and air temperature for 1901–2020 (daily heavy rainfall) and 1947–2020 (hourly heavy rainfall)

	Daily heavy rainfall anomaly			Hourly heavy rainfall anomaly		
	Entire region	North	South	Entire region	North	South
Meridionality (dynamic)	**0.72 (0.02)**	**0.77 (0.02)**	-0.04 (0.87)	0.39 (0.31)	0.66 (0.07)	0.30 (0.46)
Persistency (dynamic)	**0.63 (0.04)**	0.51 (0.10)	**0.60 (0.02)**	0.31 (0.40)	0.56 (0.12)	0.25 (0.51)
Air temperature (thermodynamic)	0.22 (0.47)	0.26 (0.40)	0.26 (0.30)	**0.93 (0.03)**	**0.80 (0.05)**	**0.95 (0.04)**

P-values in brackets account for the autocorrelations of the time series[58]. Analysis separately for the entire region, north and south of the Alpine ridge. Heavy rainfall has been corrected for errors caused by the registration type, while in Table 3 it has not.

Extended Data Table 2 | Spearman's rank correlation coefficients of daily and hourly heavy rainfall (original and bias corrected) with annual flood peaks in small (<50 km²) and large (>500 km²) catchments for 1950–2022

	Daily heavy rainfall anomaly			**Hourly heavy rainfall anomaly**		
	Entire region	North	South	Entire region	North	South
Correlation between floods in **small catchments** and **original** heavy rainfall data	0.42 (0.30)	0.33 (0.41)	0.54 (0.10)	**0.92 (0.03)**	0.70 (0.08)	**0.93 (0.03)**
Correlation between floods in **large catchments** and **original** heavy rainfall data	0.62 (0.09)	0.67 (0.07)	-0.03 (0.89)	0.67 (0.07)	**0.80 (0.03)**	0.07 (0.72)
Correlation between floods in **small catchments** and **bias corrected** heavy rainfall data	0.44 (0.29)	0.36 (0.38)	0.53 (0.11)	**0.92 (0.03)**	0.71 (0.08)	**0.93 (0.03)**
Correlation between floods in **large catchments** and **bias corrected** heavy rainfall data	0.63 (0.08)	0.68 (0.07)	-0.07 (0.74)	0.67 (0.07)	**0.80 (0.03)**	0.07 (0.72)

P-values in brackets account for the autocorrelations of the time series[58]. Analysis separately for the entire region, north and south of the Alpine ridge.

Extended Data Table 3 | Scaling of heavy rainfall with respect to air temperature (%/°C)

	Daily heavy rainfall			Hourly heavy rainfall		
	Entire region	North	South	Entire region	North	South
Instantaneous scaling						
1950-2023	-0.8	-1.4	-0.5	6.8	7.8	6.5
1980-2023	-0.8	-1.4	-0.4	6.8	7.8	6.6
Climate scaling						
1950-1970 vs. 2003-2023	2.3	2.4	2.2	8.0	7.7	8.4
1980-2000 vs. 2003-2023	6.9	10.1	3.7	9.9	10.2	9.7

Instantaneous scaling for 1950–2020 and 1980–2020, and climate scaling for 1950–1970 vs. 2000–2020 and 1980–2000 vs. 2000–2020. Analysis separately for the entire region, north and south of the Alpine ridge.